Advances in Polymer Technology

Design, Synthesis, and Applications of Field-Sensitive Polymers

Lead Guest Editor: Xin Hu
Guest Editors: Liang Fang and Yin Fang

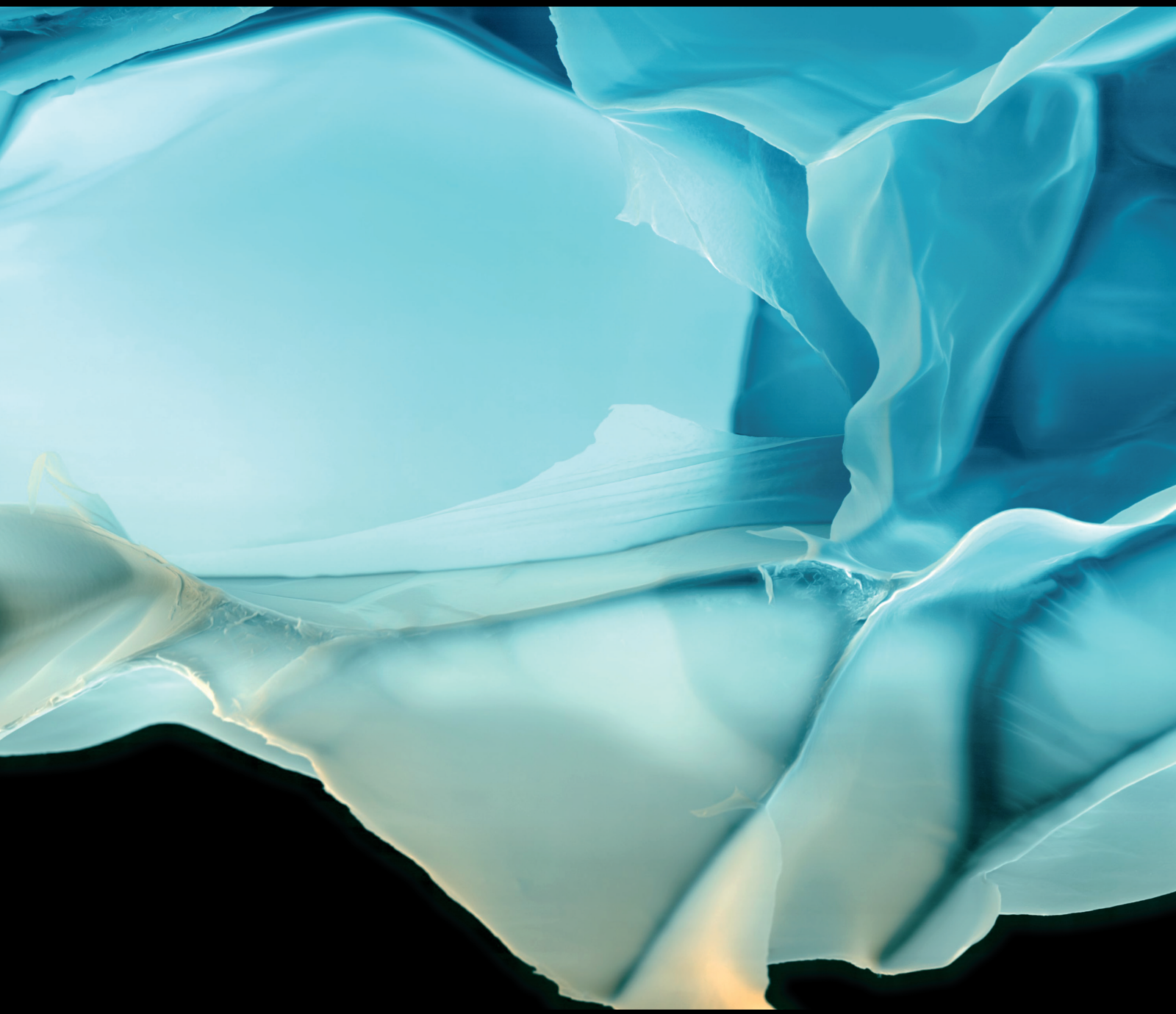

Design, Synthesis, and Applications of Field-Sensitive Polymers

Advances in Polymer Technology

Design, Synthesis, and Applications of Field-Sensitive Polymers

Lead Guest Editor: Xin Hu
Guest Editors: Liang Fang and Yin Fang

Contents

Hindawi
Advances in Polymer Technology
Volume 2020, Article ID 7639724, 16 pages
https://doi.org/10.1155/2020/7639724

Review Article

Surface Structures, Particles, and Fibers of Shape-Memory Polymers at Micro-/Nanoscale

Liangliang Cao,[1,2,3] Liwei Wang,[4] Cihui Zhou,[1,2,3] Xin Hu,[1,2,3] Liang Fang,[1,2,3] Yaru Ni,[1,2,3] Chunhua Lu,[1,2,3] and Zhongzi Xu[1,2,3]

[1]*State Key Laboratory of Materials-Oriented Chemical Engineering, College of Materials Science and Engineering, Nanjing Tech University, Nanjing 210009, China*
[2]*Jiangsu Collaborative Innovation Center for Advanced Inorganic Function Composites, Nanjing Tech University, Nanjing 210009, China*
[3]*Jiangsu National Synergetic Innovation Center for Advanced Materials (SICAM), Nanjing Tech University, Nanjing 210009, China*
[4]*Beijing Institute of Space Launch Technology, Beijing 100076, China*

Correspondence should be addressed to Xin Hu; xinhu@njtech.edu.cn, Liang Fang; lfang@njtech.edu.cn, and Chunhua Lu; chhlu@njtech.edu.cn

Received 1 July 2019; Accepted 6 December 2019; Published 8 January 2020

Academic Editor: Behnam Ghalei

Shape-memory polymers (SMPs) are one kind of smart polymers and can change their shapes in a predefined manner under stimuli. Shape-memory effect (SME) is not a unique ability for specific polymeric materials but results from the combination of a tailored shape-memory creation procedure (SMCP) and suitable molecular architecture that consists of netpoints and switching domains. In the last decade, the trend toward the exploration of SMPs to recover structures at micro-/nanoscale occurs with the development of SMPs. Here, the progress of the exploration in micro-/nanoscale structures, particles, and fibers of SMPs is reviewed. The preparation method, SMCP, characterization of SME, and applications of surface structures, free-standing particles, and fibers of SMPs at micro-/nanoscale are summarized.

1. Introduction

Shape-memory polymers (SMPs) are capable to be deformed and fixed into temporary shapes as well as to recover toward their original/permanent shapes upon external stimuli including heat, light, pH, electric field, and magnetic field [1–4]. In the last two decades, SMPs have attracted great attention from both academic and industrial fields because they can be used in biomedical devices, aerospace, smart textile, soft actuators, flexible electronics, and so on [5–12]. Shape-memory effect (SME) is not a unique ability for specific polymeric materials but results from the combination of suitable molecular architecture and a tailored shape-memory creation procedure (SMCP) [13, 14]. In addition, the shape of SMPs can be programmed on-demand. These two features offer SMP advantages over other shape-changing polymers such as smart hydrogels [15–17] and liquid crystal elastomers [18–20].

The molecular architecture of SMPs mainly consists of two elements, i.e., netpoints and switching domains, which are responsible for permanent shape and temporary shape, respectively [1, 4]. Switching domains are usually contributed by glass transition, melt/crystallization, reversible connection, supramolecular bonding, and so on [21]. Netpoints can be either chemical crosslinking in the form of covalent bonds or physical crosslinking [21]. More specifically, chemical crosslinking determines the permanent shape of thermoset SMPs, and the domains having higher

transition temperature (T_{trans}) in thermoplastic SMPs, i.e., glass transition temperature (T_g) or melting temperature (T_m), act as physical netpoints [22].

The molecular mechanisms of thermoset SMPs within SMCP and recovery modules are illustrated in Figure 1. External force is first applied to deform an SMP specimen into a temporary shape at deformation temperature (T_{deform}) that is higher than T_{trans} (T_g or T_m) of switching domains, leading to the orientation of polymer chains. Subsequently, by cooling below T_g (Figure 1(a)) or crystallization temperature, T_c (Figure 1(b)), of the switching domains, the temporary strain is stored via the solidification of switching domains. When the specimen is reheated beyond the switching temperature (T_{sw}) that is dominated by T_{trans}, recovery process occurs via entropy-driven recoiling of the oriented polymer chains. If $T_{trans} = T_g$, the strain-induced nonequilibrium state is retained via the vitrification of the amorphous phase (Figure 1(a)). If $T_{trans} = T_m$, the crystallization of switching domains limits the flexibility of oriented polymer chains as shown in Figure 1(b).

The quantification of SMCP, i.e., how efficient a defined deformation can be obtained, is typically characterized by measuring the shape-fixity ratio, R_f, using the following equation [13]:

$$R_f = \frac{\varepsilon_u(N)}{\varepsilon_m}, \quad (1)$$

where $\varepsilon_u(N)$ and ε_m are strains after releasing stress at T_{low} in the N^{th} cycle and deformed strain, respectively. The recovery from the fixed shape to the permanent one during applying external stimuli is of the most importance to evaluate SME. Stress-free recovery, i.e., no external load is applied, is the most common method to quantify shape recovery. Shape recovery ratio, R_r, is typically characterized by the ratio of the strain during the present N^{th} cycle, ε_m–$\varepsilon_p(N)$, and the strain obtained during SMCP in the previous $(N-1)$ cycle, ε_m–$\varepsilon_p(N-1)$, as shown in equation (2). An additional characteristic of SME is switching temperature, T_{sw}, which is defined as the temperature where the highest recovery rate is obtained [13].

$$R_r = \frac{\varepsilon_m - \varepsilon_p(N)}{\varepsilon_m - \varepsilon_p(N-1)}. \quad (2)$$

With the development of SMPs, the trend toward the exploration of the ability of SMPs to recover structures at micro-/nanoscale occurs. Several approaches focused on the indentation of SMP films, in some cases, in combination with the subsequent removal of the topmost polymer layers [23–27]. Temporary cavities are generated onto SMP surfaces by indentation techniques, which can be erased upon annealing. However, the minimization in surface energy may also enable polymers to reach smooth surface [28]. The recovery of the indented nanostructures to permanent smooth surface, thus, may not be unique for SMPs. Another widely reported manner for demonstrating SMEs at micro-/nanoscale is to incorporate permanent micro-/nanostructures onto SMP substrates using molding replication as well as to deform them into either flat surface or other structures with different features [29–43]. Furthermore, free-standing SMP matrices with all dimensions at microscale are also of increasing interest [44–48]. These free-standing particles or fibers may behave differently from indented and micro-/nanostructured SMP surfaces because the underlying bulk material may, to some extent, contribute to their shape-memory functionality. The SMCP may involve distortion, e.g., of pillars, during which their deformation is transferred into the bulk phase. Accordingly, the underlying matrix may contribute to or even dominate the switching of surface structures. In contrast, free-standing SMP particles of fibers at micro- or nanoscale exclude the contributions of underlying bulk materials.

In this review, the recent progress in the development of micro-/nanoscale structures and particles of SMPs is discussed. We try to summarize the preparation method, SMCP, characterization of SME, and applications of SMP surface structures, particles, and fibers at micro-/nanoscale. We hope that this short review can be beneficial for developing miniature SMP devices that can be used greatly in optical, biomedicine, and smart surface areas.

2. Surface Structures of SMPs at Micro-/Nanoscale

2.1. Preparations of Permanent SMP Surface Structures at Micro-/Nanoscale. The reported SMP systems as well as the prepared features and aspect ratio (AR) of the micro-/nanostructured surfaces are briefly summarized in Table 1. Based on feature dimensions, permanently 2D, 2.5D, and 3D structures on SMP surface can be considered [49]. Typically, 2D structures present elongated features in surface plane such as groove patterns, while 2.5D structures present uniformly spacing features with the same geometry in the vertical direction such as cylindrical pillar arrays. The features with variable geometry in the vertical direction can be considered as 3D structures such as microprism and microlens arrays [49].

For the reported SMP-structured surfaces, 2D and 3D structures have a small AR (≤1) [32, 33, 50–55], while 2.5D structures possess a relatively high AR (≥1) [29–31, 56]. The main method to create permanent SMP-structured surface is to enable the replication of polymer or prepolymer surface from master molds (Table 1). As shown in Figure 2(a), a mold with pre-defined microstructures is placed against the SMP surface at a high temperature under load, allowing the sufficient filling of materials into mold cavities. The embossed specimens are subsequently cooled down in the presence of the load. A structural replication of SMP surface from the master mold is achieved after the mold is released. This method is quite efficient for thermoplastic SMPs with good flowing capability at the high temperature [55, 57]. For example, the 2.5D pillar arrays with AR = 4 of a thermoplastic polyurethane (Tecoflex, having a wide range of T_g ending at 120°C–140°C) were successfully fabricated at 200°C [57].

After the formation of covalent network, the mobility of crosslinked polymers into mold cavities is limited. Therefore, to facilitate chemically crosslinked SMPs to fully

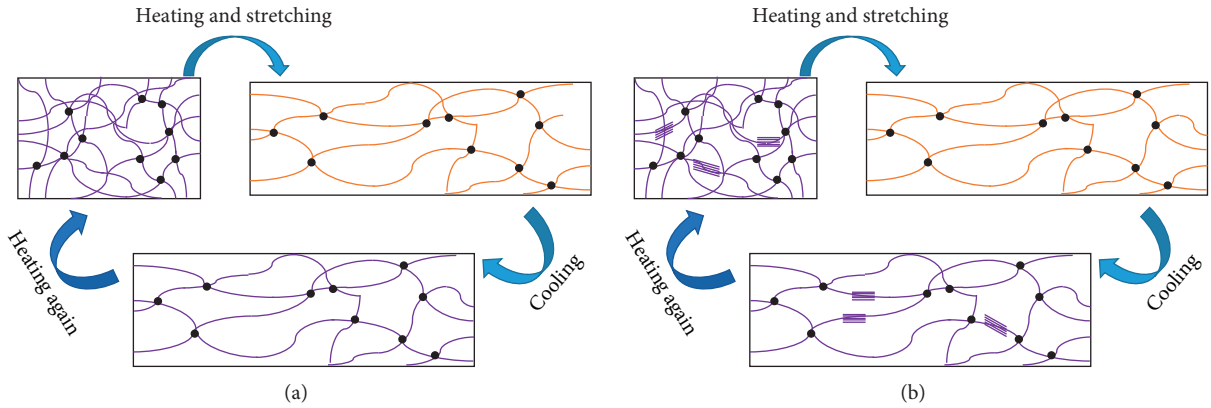

FIGURE 1: Schematic illustration of the molecular mechanisms of SMPs having chemically crosslinked netpoints during SMCP and recovery modules. In system (a), $T_{trans} = T_g$, and in system (b), $T_{trans} = T_m$.

replicate the master mold, prepolymers (polymer and curing agent) are typically used instead [32, 50, 53, 56]. As shown in Figure 2(b), after imprinting the mold against premixed prepolymers, extra thermal curing or photocuring step is performed to generate chemical networks of SMPs in mold cavities. Crosslinked poly(ε-caprolactone) (c-PCL) is the widely reported thermosetting SMP system to produce SMP-microstructured surfaces, the network of which is generated through either thermal curing or photocuring [32, 50, 56]. Via crosslinking tetra-branched PCL with acrylate end-groups in the presence of linear PCL telechelic diacrylate, 2D groove patterns of c-PCL with $T_{sw} = 33^{\circ}C$ were generated [32]. With the aid of benzoyl peroxide as the cuing agent, allyl alcohol-plasticized PCL was crosslinked at 130°C, thereby generating 2.5D pillar arrays with AR = 3 and $T_{sw} = 37–46^{\circ}C$ [56]. Finally, as an instance, PCL networks with $T_{sw} = 40^{\circ}C$ were prepared by photocuring PCL trimethacrylate in the presence of diethoxyacetophenone as photoinitiator [50].

Utilization of precursors is another approach to efficiently create 2.5D SMP microstructures having high AR [30, 31]. As shown in Figure 2(c), instead of placing a mold against SMP surface, precursors with low viscosity are poured into the mold before thermal treatment is performed to cure the materials. Because polymer microstructures with high AR possess large surface area and adhesion force, they are liable to mechanical instabilities, such as lateral and ground collapses [31]. The critical aspect ratio (AR_c) for lateral and ground collapses can be calculated using the Equations as follows:

$$AR_c = \frac{0.49\pi^{1/3}E^{1/3}S^{1/2}}{W^{1/3}d^{1/6}(1-\nu^2)^{1/12}},$$
$$AR_c = 0.284\left(1-\nu^2\right)^{1/6}\left(\frac{Ed}{W}\right)^{2/3}, \quad (3)$$

where E, W, ν, and d stand for Young's modulus, adhesion work, Poisson's ratio, and diameter of the pillar, respectively, while s is pillar-to-pillar spacing [31]. An epoxy-based SMP, as an instance, resulted from the thermal curing of diglycidyl ether of bisphenol A (DGEBA) and poly(propylene glycol) bis(2-aminopropyl ether), and decylamine has been used to create pillar arrays with AR = 2–4 [31]. For such pillars having diameter of 10 μm, the AR_c for lateral collapse increased from 4.9 for $s = 5\,\mu m$ to 12.0 for $s = 30\,\mu m$, while the AR_c for ground collapse remained as 28.0 [31].

Last but not the least, nanoimprint lithography (NIL) offers a simple approach to fabricate nanostructures onto the SMP surface by creating a polymer sacrificing layer, onto which SMP precursors can be poured and cured before the sacrificing layer is removed afterwards [51]. As an example, polyacrylic acid (PAA) nanopatterns on silicon wafers were first created via thermal embossing NIL. The curing of acrylate-based SMPs precursors on nanostructured PAA layer was then performed. After dissolving the sacrificing PAA layer, the SMP-nanostructured surfaces with identical 2D groove pattern having the height of 20–194 nm were obtained [51].

2.2. SMCP of SMP Surface Structures at Micro-/Nanoscale. In comparison with the macroscale, SMCP at micro-/nanoscale is challenging. In brief, the demonstrated approach to program SMPs micro-/nanostructured surface is applied to a vertical load to compress the structures with AR <1 or a shearing force to tilt the structures with AR <1, using a flat or structured plate. During SMCPs, permanent SMPs-micro-/nanostructured surfaces are deformed into temporary structures having required features relative to the applications. Permanently flat SMP surfaces are usually deformed into temporarily 2D groove patterns for cell culture [32, 50, 55, 58]. As an instance, permanently flat surface of NOA-63 (a polyurethane with ends linked by thiol-based crosslinker) was compressed by an epoxy embosser at 90°C for 1 min, before 5 min of cooling at 20°C under the compression [58]. The microstructures can be easily erased, i.e., recover to the previously flat surfaces, upon heating above T_{trans}.

Permanent 2D and 3D structures with AR <1 are typically deformed into flat surfaces or other features via compression or imprinting for applications in the fields of

Table 1: Material systems with their switching temperatures and curing methods, as well as structural features, geometries, and aspect ratios of reported SMP-micro-/nanostructured substrates.

Material system	T_{sw}	Curing methods	Structural dimensions and features	Geometries	AR	Ref.
Polymers						
Polynorbornene; pristine fullerenes		N.A.	3D nanolens arrays	$H = 250$ nm $D = 250$ nm $S = 250$ nm	1	[55]
Tecoflex 72D : cycloaliphatic polyetherurethane block copolymer	51	N.A.	2.5D pillar arrays	$H = 100\ \mu$m $D = 20\ \mu$m $S = 20\ \mu$m	5	[57]
Prepolymers						
PCL trimethacrylate; diethoxyacetophenone	40	Photo	3D Hexnuts Boomerangs	$3\ \mu\text{m} \times 1\ \mu$m $10\ \mu\text{m} \times 1\ \mu$m		[50]
NOA-63 : a polyurethane which is end-linked by a thiol-base crosslinker using photoinitiated thiol-ene crosslinking	Altered	Photo	2D Groove patterns	$H \sim 9.2\ \mu$m $W \sim 140\ \mu$m $S \sim 140\ \mu$m	0.06	[58]
Tetra-branched PCL with acrylate end-groups Linear PCL telechelic diacrylates	33	Thermo	2D groove patterns	$H = 150$ nm $W = 1\ \mu$m $S = 2\ \mu$m	0.15	[32]
Poly(ethylene-co-vinyl acetate); dicumyl peroxide	63	Photo	3D Microprism array, microlens arrays, white-light hologram, transmission grating	For microprism $H = 72\ \mu$m $W = 150\ \mu$m	0.5	[53]
Linear PCL Allyl alcohol Benzoyl peroxide	37–46	Thermo	2.5D Pillar arrays	$H = 15\ \mu$m $D = 5\ \mu$m $S = 5\ \mu$m	3	[56]
Precursors						
Bisphenol a diglycidyl ether (BADGE); poly(propylene glycol) bis(2-aminopropyl ether); decylamine	60	Thermo	2.5D pillar arrays	$H = 4\ \mu$m $D = 1\ \mu$m $S = 1$ or $2\ \mu$m	4	[30]
Bisphenol a diglycidyl ether (BADGE); poly(propylene glycol) bis(2-aminopropyl ether); decylamine	60	Thermo	2.5D pillar arrays	$D = 10\ \mu$m $S = 5$–$30\ \mu$m	2–3	[31]
Diglycidyl ether of bisphenol: an epoxy monomer; *m*-xylylenediamine; *n*-octylamine	78	Thermo	2.5D pillay arrays	$H = 10\ \mu$m $W = 10\ \mu$m $S = 5, 10, 20, 30\ \mu$m	1	[40]
Diglycidyl ether of bisphenol: an epoxy monomer; poly(propylene glycol) bis(2-aminopropyl ether); neopentyl glycol diglycidyl ether	35–65	Thermo	3D pyramids-termed microtips	$H = 12$–$21\ \mu$m $W = 17$–$30\ \mu$m $S = 100\ \mu$m	0.7	[52]
Methyl methacrylate; poly(ethylene glycol dimethacrylate); photoinitiator	95	Photo	Groove patterns	$H = 194$ nm $W = 834$ nm $S = 834$ nm	0.2	[51]

H: height; W: width; D: diameter; S: spacing

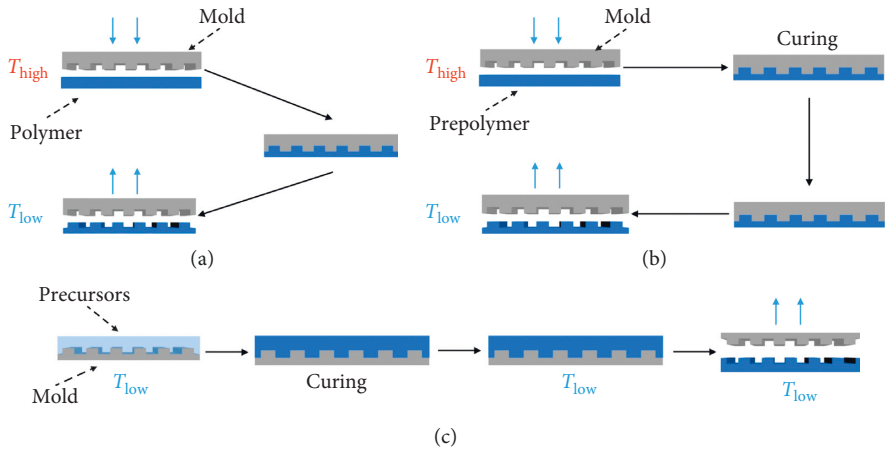

FIGURE 2: Schematic illustration of preparation methods of permanent SMP-structured surfaces from (a) polymers, (b) prepolymers (polymer + curing agent), and (c) polymer precursors.

micro-optical devices, dry adhesion, or microchannels [29, 33, 50–53]. By compressing against a flat quartz substrate at 105°C for 5 min, 3D microprism arrays of cross-linked poly(ethylene-co-vinyl acetate) (cPEVA) were distorted during SMCP before the sample was cooled down to room temperature in the presence of the compression force [53]. Similarly, the programming of 2D groove nanopatterns of an acrylate-based SMP into flat surface was carried out using NIL with a flat wafer at 180°C for 30 min [52]. Besides, the SMCP of microstructures into flat surfaces can be directly performed for certain applications in dry adhesion. Uniformly spaced microscale 3D pyramids-shaped microtips of thermoset epoxy-based SMP were placed against a mating substrate at the temperature above its T_g, resulting in the collapse of microstructures into flat surfaces as shown in Figure 3. The contact with the substrate was maintained after cooling below its T_g [52]. In addition to programming micro-/nanostructured substrates into flat surfaces, they were also deformed into different features [33, 50]. The c-PCL surfaces with 3D hexnuts and boomerang structures at microscale were mechanically deformed to cubic and cylindrical arrays at 130°C using a second replica mold and subsequently cooled to −78°C under the load [50]. Furthermore, the c-PCL films with permanent 2D linear and *L*-shaped channel patterns, as a potential application in microfluidic control, were overwritten above T_m for 5 min by the same structures oriented perpendicular to the permanent ones, before the temporary shapes were fixed at 4°C for 10 min [33].

The permanent 2.5D structures having a high AR >1 are typically inclined and compressed to control the adhesion ability and contact angle of the surface as well as to govern cell behaviors [29–31, 57]. Pillar arrays of a thermoplastic elastomer (Tecoflex 72D), having a high AR = 5, were heated above T_{trans}. A glass plate was utilized to press smoothly against the pillars before pulling it manually along specific directions (Figure 4) [57]. In the presence of the glass plate, the sample was cooled down below T_{trans} to fix the deformation. A tilting angle of 45° was typically obtained. Similar creation procedures were performed to shear epoxy-based SMP pillar arrays with AR = 2–3 at 80°C along the lattice vector and diagonally along the lattice. In addition to tilting, two sets of identical pillar arrays with a high AR were pressed against each other at 80°C (above T_g) and subsequently cooled down to room temperature to fix the deformed shape (Figure 5) [30]. The deformed scenario, including interdigitation, indenting, and interweaving highly depended on load, pillar geometries (diameter, spacing, AR), and elastic modulus of the material at T_{deform}.

2.3. Recovery Manner and Quantification of SMP Surface Structures at Micro-/Nanoscale. The incorporation of different stimuli resources, multiple shape transitions, and reversibility into SMP structures at micro-/nanoscale results in more functions and thereby explores more potential applications. In addition, similar to SMCP at micro-/nanoscale, the quantification of SMEs at micro-/nanoscale is also challenging. New evaluation methods are required based on offline microscopic approaches and measurement parameters.

To date, the research on SMP-micro-/nanostructured surfaces mainly focuses on the area of direct thermally-induced one-way dual-shape memory effect, i.e., upon heating, the programmed temporary shape recovers to the permanent shape directly, which cannot return to the temporary shape again without another SMCPs [30, 32, 52]. Recently, studies on indirect thermally-induced one-way dual-shape memory effect [55], direct thermally-induced one-way multiple-shape memory [3], and direct thermally-induced two-way reversible multiple-shape memory effect [54] have been involved as well. Therefore, in this context, we present these recent developments of SMP-micro-/nanostructured surfaces before the discussion of quantifying the SMEs.

Instead of heating, the recovery of deformed nanolens arrays of polynorbornene with 0.1 wt% fullerene was triggered by absorbing electromagnetic energy which was generated by microwave irradiation [55]. The fullerene as a thermal conductive filler played a role in absorbing microwave and reinforcing the nanostructures simultaneously,

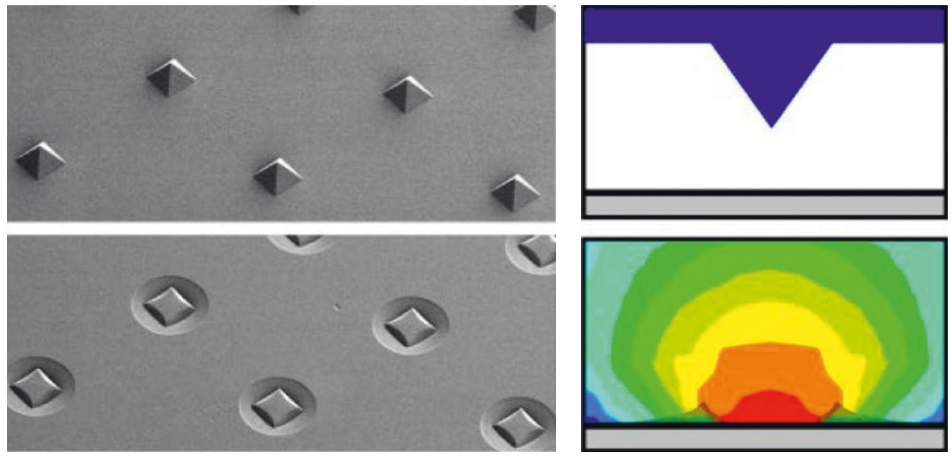

Figure 3: Schematic illustration of the programming of SMP microtips against flat substrate and the subsequent recovery. This figure was modified from [52].

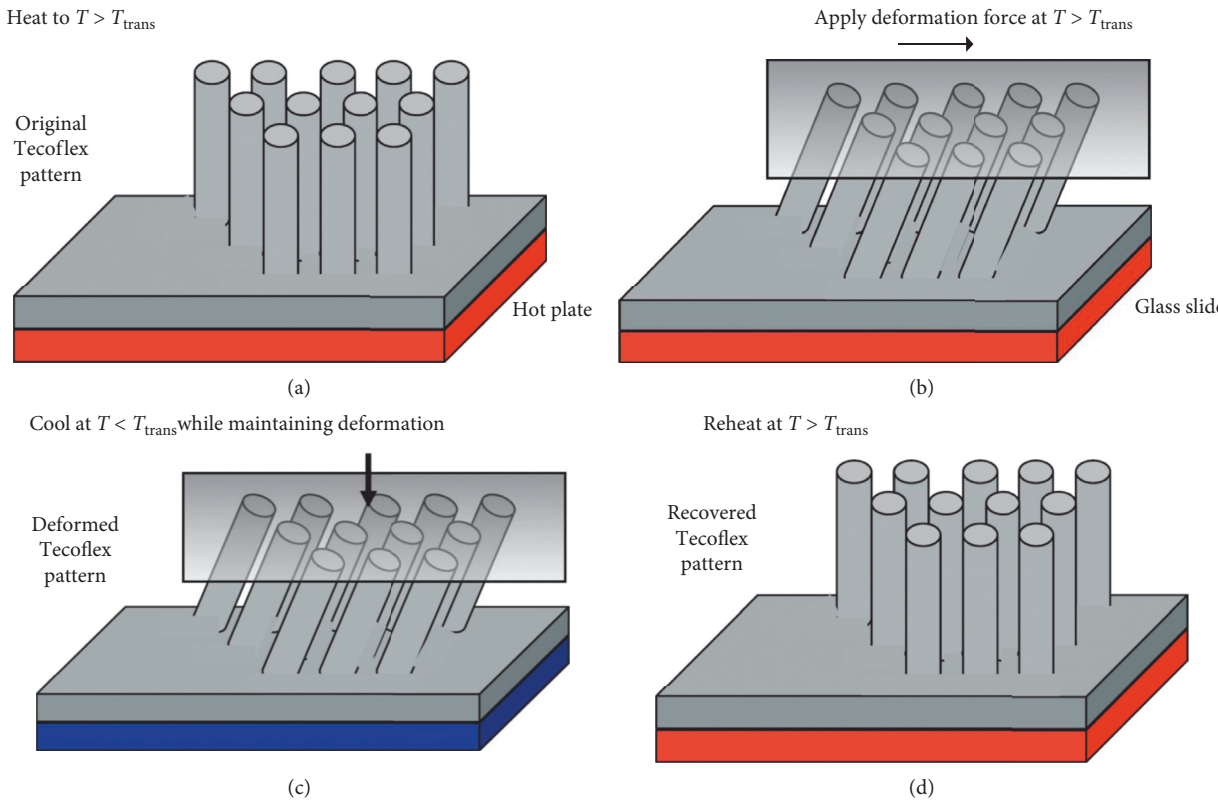

Figure 4: The inclining deformation of Tecoflex SMP pillar arrays during SMCP and the subsequent recovery. This figure was modified from [57].

realizing the indirect thermally-induced one-way dual-shape memory effect of microstructured surfaces.

Nafion is a perfluorosulphonic acid ionomer having a broad T_g from 55 to 130°C, which has been reported presenting dual-, triple- and at least quadruple-shape memory effects [3]. Its triple-shape memory effect has also been achieved in the nanostructured surfaces [51]. As shown in Figure 6, the permanent Nafion film with groove patterns ($H = 194$ nm, $s = 834$ nm, Figure 6(a)) were programmed into grid-like patterns at 90°C for 3 min (Figure 6(b)), before another silicon wafer ($s = 150$ nm) was pressed against Nafion sample oriented 45° with respect to the previous groove patterns at 60°C for 30 min (Figure 6(c)). Upon heating at 60°C for 80 min, the second temporary shape (pattern with $s = 150$ nm) almost disappeared (Figure 6(d)). Subsequently annealing Nafion film at 90°C for 10 s, the

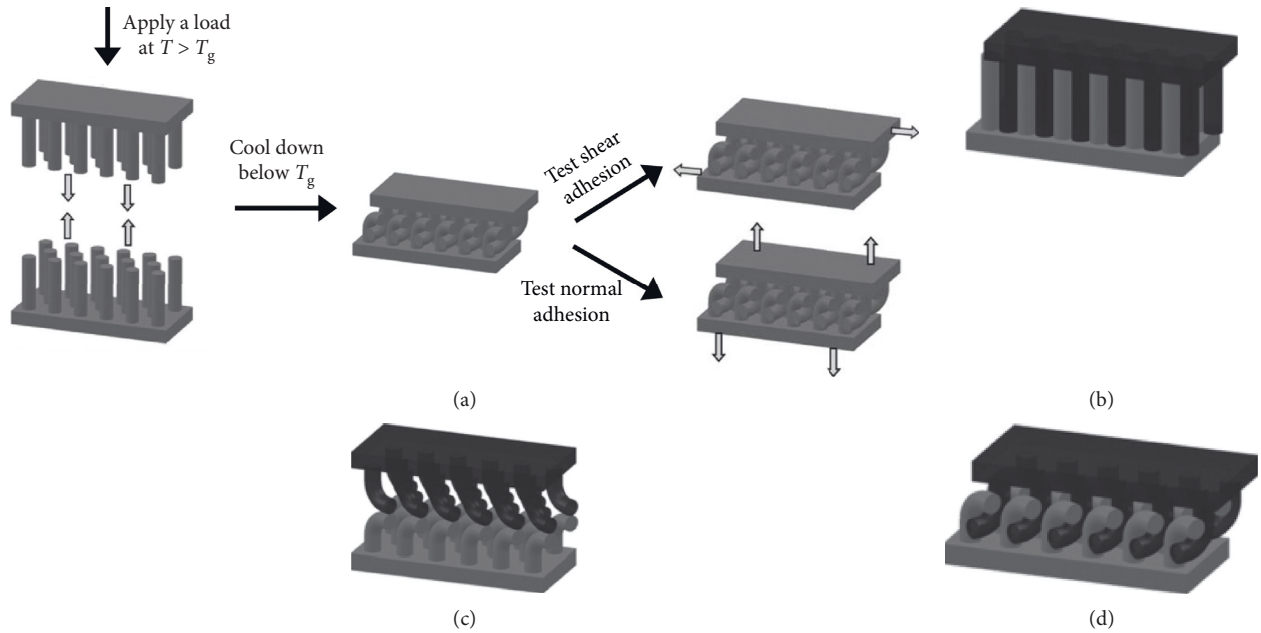

FIGURE 5: (a) Schematic diagram of pressing identical pillar arrays against each other as well as the adhesion measurements. (b–d) Three possible deformation modes between two identical pillar arrays after SMCP: (b) interdigitation, (c) indenting, and (d) interweaving. This figure was modified from [30].

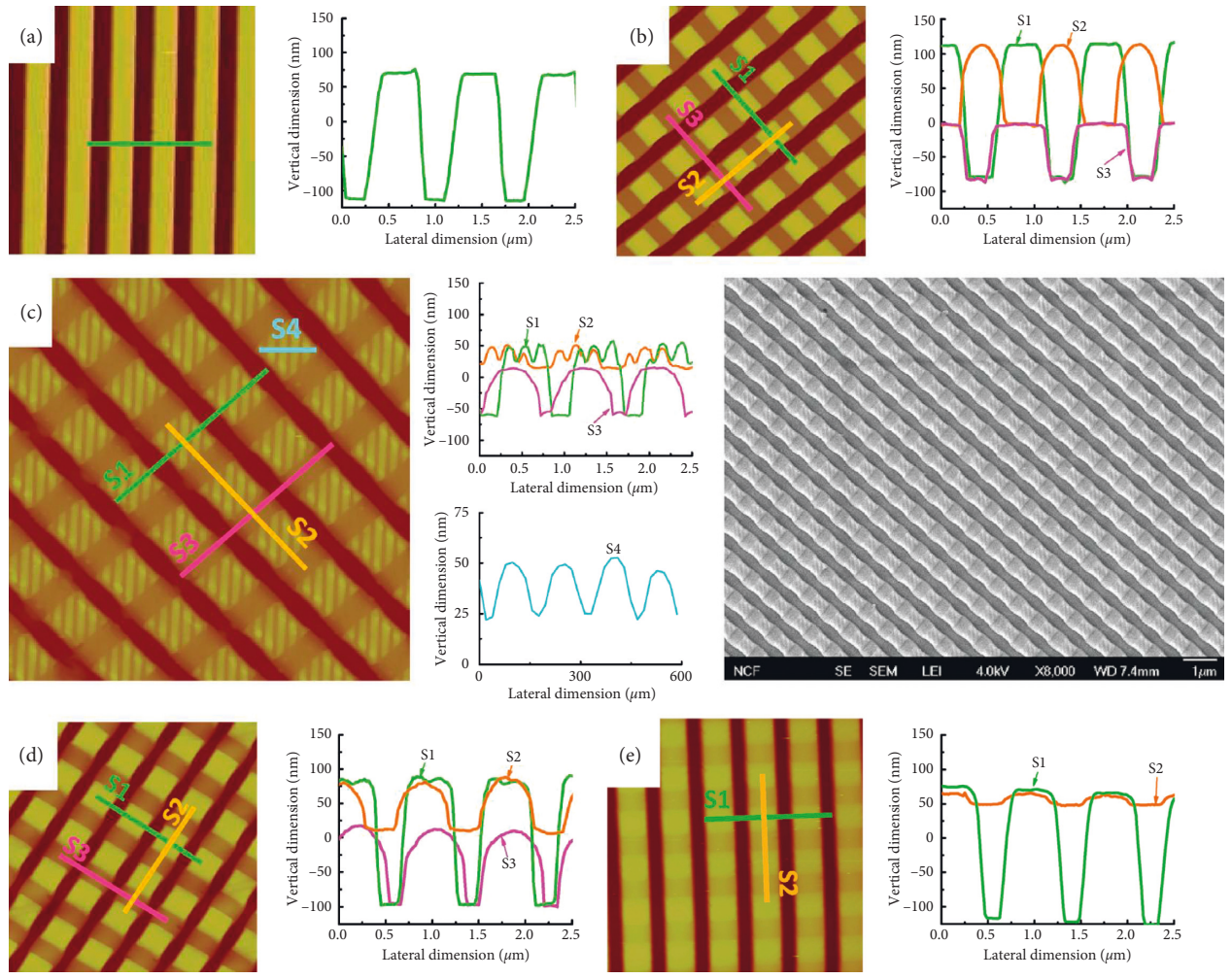

FIGURE 6: Topographic AFM images of multipattern memory effect in Nafion films programmed by TE-NIL. This figure was modified from [51].

permanent groove patterns were obtained again (Figure 6(e)).

The two-way multiple-shape memory effect of the thermosetting copolyester poly(octylene adipate)-*co*-poly(octylene diazoadipate) sub-microstructured surfaces has been reported [54]. When the temporary flat surfaces were heated to an intermediate temperature of 50°C, partial melting of crystals allowed the shape recovery toward the permanent boomerang patterns, increasing the feature height. Cooling from the intermediate temperature to 20°C resulted in the recrystallization and reversion toward the temporary flat surfaces. Therefore, the feature height was reduced again. Variations in one heating and cooling cycle (20–50°C) caused the height change in the range of 60–70 nm.

Furthermore, the full recovery of pillar arrays having high AR has been reported to be dependent on the adhesion energy between neighboring pillars, which was affected by pillar spacing [30, 31]. Upon heating, simultaneous and uniform recovery of inclined pillar arrays can be achieved on the square lattice with $s = 30\,\mu$m. However, at the hexagonal lattice with $s = 10\,\mu$m, the recovery was localized because the pillars were in lateral contact. Similarly, if two identical sets of pillar arrays were pressed against each other, only when the adhesion energy between interweaved or indented pillars were small, and the full recovery of pillar arrays can be achieved. Therefore, the collapsed pillar arrays with $\alpha = 2$ cannot recover at all, while at $\alpha = 3$, pillars partially recovered upon heating.

The full quantification of SME of micro-/nanostructured polymer surfaces, i.e., the determination of R_r, R_f, and T_{sw}, is a challenge. To date, most research is limited in the evaluation of R_r based on the height variation of the vertically deformed 2D and 3D structures or the angle change of the inclined 2.5D structures [32, 33, 51, 57]. The recovery ratio of 2D groove patterns made of acrylate-based SMP was quantified using the following equation:

$$R_r = \frac{H_{recovered}}{H_{permanent}}, \tag{4}$$

where $H_{recovered}$ and $H_{permanent}$ are recovered and permanent heights of the grooves, which can be obtained from the cross-section profile of the atomic force microscopy (AFM) topography images [51]. The full-pattern recovery was achieved for all patterns having different $H_{permanent}$ from 20 to 179 nm [51], suggesting that the size limitation of SME on structured surfaces could be reduced down to sub-100 nm. The recovery of 2.5 D pillar arrays made of a shape memory thermoplastic elastomer (Tecoflex 72D) was quantified as follows:

$$R_r = \frac{\theta_{temporary} - \theta_{recovered}}{\theta_{temporary} - \theta_{permanent}}, \tag{5}$$

where, θ represents pillar tilting angles in original ($\theta_{permamemt} = 90^\circ$), deformed ($\theta_{temporary}$~44°), and recovered ($\theta_{recovered}$~75°) positions, measured from electronic scanning microscopy images [57]. A partial recovery, i.e., $R = 67\%$, was obtained after the first deformation because the overload applied for the tilting could result in the permanent deformation [57]. In addition to direct measurements of the geometry variation during recovery, the transmittance of cPEVA film varied during recovery, which was related to the height variation of the microprism arrays, was also used to indirectly evaluate the recovery ratio, i.e., $R_r = I_{recovered}/I_{original}$ [53]. Here, $I_{recovered}$ and $I_{original}$ stand for the light transmittance through the recovered and original films. R_r of 100% was observed, suggesting a complete microstructure recovery [50].

2.4. Applications of SMP Surface Structures at Micro-/Nanoscale. Upon applying the stimuli, the temporarily deformed structures recover to their permanent shapes, varying surface topography and thereby changing surface properties. Therefore, SMP-micro-/nanostructured surface can be used for cell culture substrates, switchable valves, and channels in microfluidics, dry adhesion, as well as micro-optics.

Cell culture substrates with defined structures are powerful tools to direct cell alignment, adhesion, and traction forces. SMP-structured substrates that enable the switch of surface structures have been reported as a new approach to provide dynamic topography to control cell behavior [32, 50, 56, 58]. The recovery force generated during the change in surface topography can be controlled more simply and precisely to examine cell behaviors by mimicking natural cellular environments [56]. It was demonstrated that the recovery of 2D groove patterns made of polyurethane-based SMP toward flat surfaces decreased the alignment of C3H/10T1/2 mouse embryonic fibroblasts, while the cell viability was not affected by the topography variation [58]. Similar results were also reported for human mesenchymal stem cells that switched from highly aligned to stellate-shaped morphology in response to the topography recovery from 2D groove patterns to flat surfaces [50]. Furthermore, 2.5D pillar arrays of allyl alcohol-plasticized crosslinked PCL-Fe_3O_4 nanocomposites, which can recover from a fully titled state at 32°C to the permanent 90° at 41°C, effectively influenced the adhesion, spread and alignment of rat bone marrow mesenchymal stem cells as well [56]. The recovery force and the variation in cell contact area provide complex mechanical environmental conditions for cells and trigger the process named as signal transduction, activating many signaling pathways and affecting their behaviors [56].

SMP-microstructured surfaces can also find themselves in the application of switchable and dry adhesions [30, 52, 57, 59]. To mimic the ability of attachment pads of lizards that can switch the reorientation of setae shaft angle and adjust the adhesive contact through a noncovalent interactions, 2.5D pillar arrays with a AR = 5 were produced from Tecoflex and programmed into tilted positions of 45° [57]. The adhesion force presented by the permanent vertical pillars was the highest (29.7 kPa), while that of the temporary deformed pillars was neglected. After the full shape recovery of the pillars to the titled positions at 75°, the adhesion force was restored (11.8 kPa), suggesting that SMP microstructures enabled a switchable adhesion. The interlocking

adhesion mechanism was also achieved by deforming two sets of identical 2.5D SMP pillar arrays with high AR against each other [30]. The pillar-pillar adhesion forces in both normal and shear manners were higher than the forces between pillars and flat surface as well as flat surface against flat surface. More importantly, the SMP offered an easy detachment, i.e., P and S dropped significantly to 4 and 8 N cm^{-1} because of the shape recovery and the modulus drop via heating to 80°C. In addition, 3D microtip arrays of SMP were pressed against a glass substrate directly, while the fixation of the microstructures provided a strong dry adhesion of 184 N cm^{-1}, which reduced to $\sim 3 \times 10^{-3}$ N cm^{-1} after the recovery at 90°C [52].

Surface topography plays a dominant role in determining surface wettability. SMP-microstructured surface, thus, enables the control of topography variation thereby tuning wettability [31, 54]. The deformed and original/recovered SMP 2.5D pillar arrays presented distinct water contact angle and droplet sliding angle. Recently, the polymer-microstructured surface having reversible SME has been used to demonstrate the modulation of wetting properties [54]. The elbow, boomerang, and cubic structures in their programmed states displayed the glycerol contact angle of ~80° at room temperature [31]. By increasing the temperature to 50°C, the structure height was increased. The contact angle, thus, was increased to 96°~105°. The cooling of the microstructured surface to 20°C decreased the reversible topography and accordingly reduced the contact angle back to 83°~88°.

The applications of SMPs for flexible, programmable, and shape-memorizing micro-optical devices have also been demonstrated [29, 51, 53]. The cPEVA film having microprism arrays that acted as a retroreflector for light that entered from the flat side of the film was programmed into flat surface that eliminated such reflection mechanism and thus made the film transparent [53]. The transmittance was increased from <0.8% for the original/recovered microprism arrays to >60% for the temporary state, as shown in Figure 7. An alternative approach to harass the microprism arrays for the purpose of tuning the transmittance was to stretch the films. As the strain increased from 0% to 400%, the transmittance increased from 0.8% to 18%. Furthermore, the deformed SMP-microstructured surfaces were heated by the arrays of transparent-resistive microheaters, selectively triggering the local recovery of the surface structures and providing additional capabilities in user-definable optics [53].

3. SMP Particles at Micro-/Nanoscale

3.1. Preparation of SMP Particles at Micro-/Nanoscale. The preparation of polymer particles at micro-/nanoscale is a routine topic of polymer science and technology [60–64]. Here, we only focus on the reported preparation method for polymer particles at micro-/nanoscale with SME. When mixing polymer droplets as one phase in an immiscible second phase, polymer micro-/nanoparticles can be found. A PPDL-PCL multiblock copolymer comprising poly(ε-caprolactone) (PCL) and poly(ω-pentadecalactone) (PPDL) segments was dissolved in methylene chloride, and the solution was dispersed in aqueous solutions of different stabilizers [45, 46]. The shear forces during the dispersion determined the particle size, and microparticles can be achieved by solvent evaporation using magnetic stirring for 3 h. Spherical particles of photocrosslinked polymer networks with six-arm poly(ethylene glycol)-poly(ε-caprolactone) were also prepared using the oil-in-water emulsion technique [65]. Electrospraying technique was also used to create microparticles of SMPs consisting of poly(ε-caprolactone) (PCL) and poly(*p*-dioxanone) (PPDO) segments [66]. The applied high electric field deforms the liquid meniscus at the nozzle tip. The liquid meniscus forms a conical jet and further breaks into droplets due to electrostatic force. Processing parameters can be easily optimized to control the size and distribution of droplets.

Nonspherical SMP particles were prepared using templating methods as well [47, 67]. A general technique, Particle Replication in Nonwetting Templates (PRINT), was introduced to fabricate monodisperse particles having complex shapes [68, 69]. The only difference between the "PRINT" process and the imprint lithography that can be used to create permanent or temporary structures on SMP surface is that the precursors do not wet the substrate. The precursors, thus, dewet from the substrate and accumulate in mold cavities. Particles with complex shapes can be achieved after curing and being isolated. Poly(ε-caprolactone) (PCL)- and poly(octylene adipate-co-meso-2,5-diazoadipate)-based SMP particles were created using this method, and the shapes included cubes, cylinders, boomerangs, and H-shapes [67]. A similar approach was also reported [47]. Instead of autonomous dewetting, the remaining crosslinked film on the mold surface was removed using a tweezer [47]. The cube-shaped microparticles of poly(ethylene-*co*-(vinyl acetate)) were transferred to a glass slide.

3.2. SMCP of SMP Particles at Micro-/Nanoscale. Because it is a big challenge to program a single SMP particle practically, there is a need to achieve SMCP onto multiple SMP microparticles simultaneously. Lendlein and coworkers suggested an approach by embedding free-standing SMP particles in the matrix consisting of water-soluble polymers [45, 46]. As shown in Figure 8, the subsequent deformation, usually stretching, of the polymer matrix with embedded SMP particles varied their original spherical shape to temporary ellipsoid shape. The deformed particles can be removed by dissolving the polymer matrix in water. To date, this approach has been used by different groups as SMCP for different polymer particles [65, 70]. Poly(vinyl alcohol) (PVA) is soluble in water and has a high melting temperature, which is one candidate matrix material for SMCP of polymer particles. Pristine PVA, however, is brittle to be handled at room temperature. Plasticizer (usually glycerol) should be used to reduce the modulus of PVA during SMCP [45, 46].

Compression of SMP particles into temporary-compressed flat particles was widely used as well [47, 66, 71]. For spherical SMP particles, Zhang et al. applied a pressure of 100 or 0.2 MPa for 10 min to compress heated SMP particles into either a

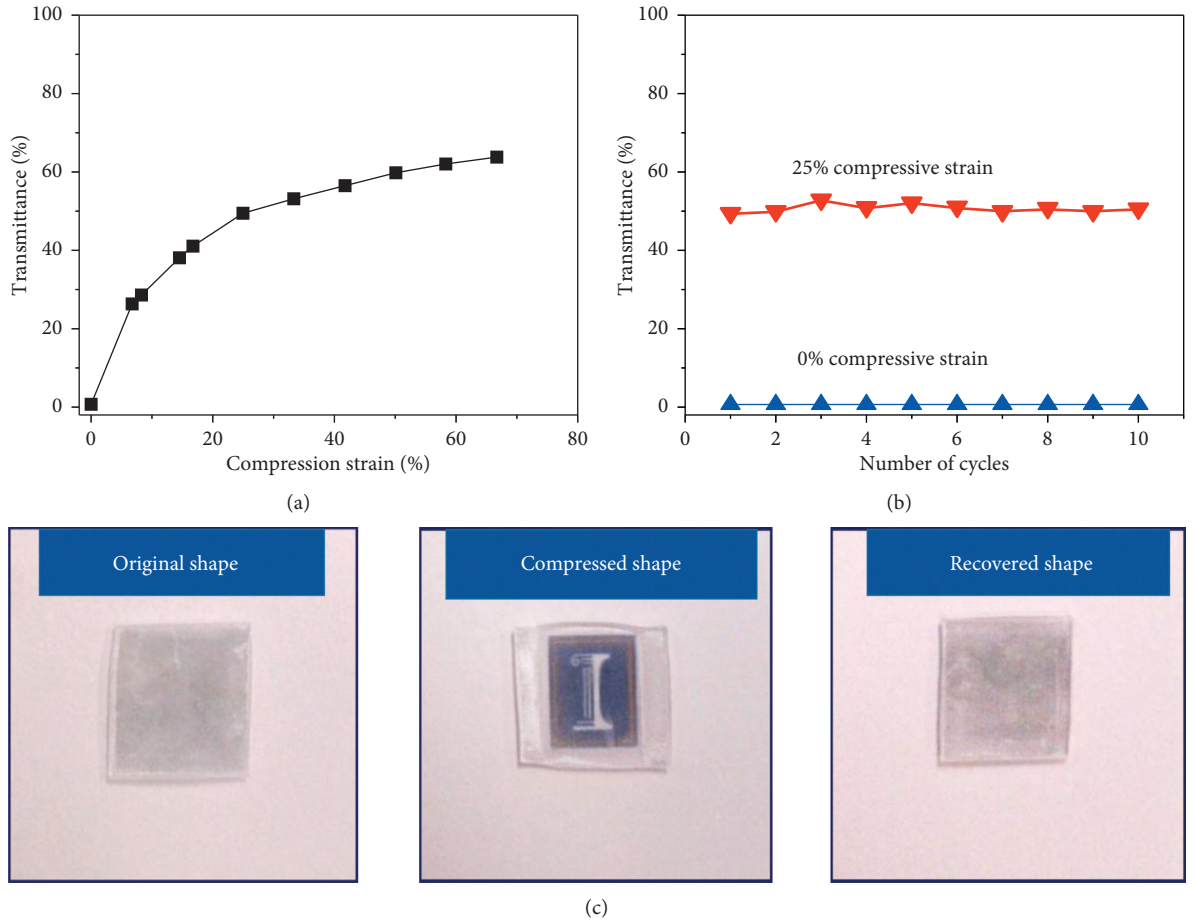

Figure 7: Transmittance variable soft films based on shape-memory polymers with programmable microprism arrays. This figure was modified from [53].

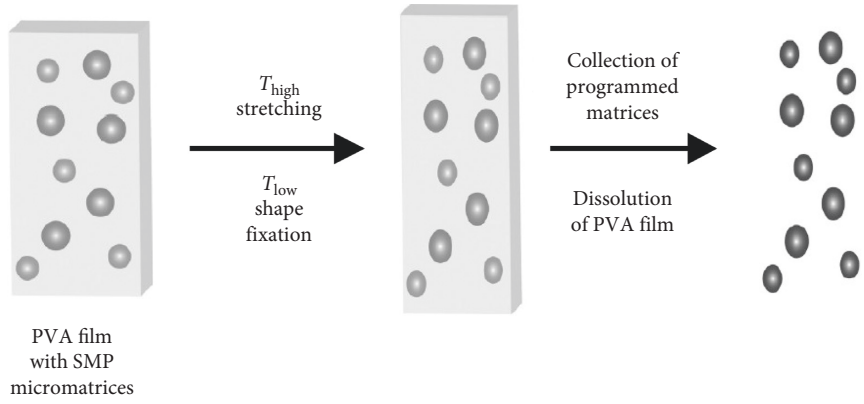

Figure 8: Schematic diagram of SMCP of SMP microparticles to a prolate ellipsoid shape followed by subsequent particle collection. This figure was modified from [45].

cylinder (100 MPa) or a partial sphere geometry (0.2 MPa) [66]. The temperature was decreased by maintaining the pressure constant. The SMCP was finished by finally removing the pressure. Liu et al. performed the similar SMCP on microcuboids using microscopy glass slides [47]. The microcuboids on the first glass slide were heated and covered by the second glass slide. Foldback clips were mounted on the two glass slides for compression. After cooling, the SMCP was finished by removing the clips and the top cover slide.

3.3. Recovery Manner and Quantification of SMP Particles at Micro-/Nanoscale. Similarly, characterization of shape variation of SMP particles at micro-/nanoscale also depends

on microscopic techniques, i.e., scanning electric microscopy (SEM) [45–47, 66], optical microscopy (OM) [45–47, 66, 67, 72], or atomic force microscopy (AFM) [47, 66]. The *in situ* heating and observation can be easily achieved using OM and AFM. At each temperature, images containing one or multiple particles are recorded. The geometries of the particles are analyzed for quantitative characterization of SME. For spherical SMP particles that were stretched, changes in AR can be used to quantitatively describe the shape recovery of microparticles as follows [45, 46]:

$$\mathrm{AR}_{\mathrm{r,AR}} = \frac{\mathrm{AR}_{\mathrm{programmed}} - \mathrm{AR}_{\mathrm{recovered}}}{\mathrm{AR}_{\mathrm{programmed}} - \mathrm{AR}_{\mathrm{original}}}, \quad (6)$$

where $R_{\mathrm{r,AR}}$ represents recovery ratio of the aspect ratio, $\mathrm{AR}_{\mathrm{original}}$ corresponds to the permanent spherical shape ($\mathrm{AR} = 1$), $\mathrm{AR}_{\mathrm{programmed}}$ is AR of the temporary prolate ellipsoidal shape, and $\mathrm{AR}_{\mathrm{recovered}}$ is AR of the same particle after shape recovery, respectively. Zhou et al. prepared polymer microparticles that can reversibly switch their shapes based on the polymer network containing six-arm PEG-PCL. The particles were deformed at 60°C using the PVA film. Reversible shape change between spherical and ellipsoid was found between 43° and 0°C [65].

The height variation during recovery is used to evaluate the SME of temporarily compressed SMP particles, including both spherical shape and cuboid shape. The recovery ratio (R_{r}) can be defined by equation (7):

$$R_{\mathrm{r}} = \frac{H_{\mathrm{r}} - H_{\mathrm{p}}}{H_{\mathrm{i}} - H_{\mathrm{p}}}, \quad (7)$$

where the initial, programmed, and recovered height of the particles are H_{i}, H_{p}, and H_{r}, respectively [47]. Liu et al. reported that the recovery ratio of microcuboids was related to the deformation ratio. They deformed microcuboids with a height of 10 μm into temporary height of 2.7 and 5.6 μm, respectively [47]. The R_{r}s were $42 \pm 1\%$ and $88 \pm 1\%$ for the one with high and low deformation, respectively. Zhang et al. compressed SMP microparticles into one free-stranding macroscopic film that disintegrated after shape recovery [66]. Smart macroscopic films that can disintegrate on demand can be envisioned.

3.4. Applications of SMP Particles at Micro-/Nanoscale. Naturally occurring particles at micro-/nanoscale including cells, bacteria, and viruses usually have nonspherical and variable shapes and can adjust their biological functions. Nowadays, more and more research studies were focused on the physicochemical properties of these stimuli-responsive micro- and nanoparticles, such as size, shape, swelling, uniformity, surface morphology, and rigidity [73–80]. Great advances in polymer microparticles have been made especially in its application in drug delivery [74, 81, 82].

The shape-switching property of SMPs can potentially provide the functions of drug delivery and medical imaging for their ability to deliver the medical molecules to the targeted locations. The shape switch under thermal stimuli often exhibit one-way characters, which is an irreversible shape changing process that the particle shape switches from a temporary shape to a permanent shape under transition temperature (T_{trans}) [83–85]. To date, SMPs with two-way effect have aroused increasing research interest in the reversible shape switch under the environment stimulus [11, 86–92]. However, two-way shape memory effect (2W-SME) materials often suffer constant stress under the cooling-heating cycles and are difficult to be carried out [86–88]. Microparticles based on biocompatible and biodegradable network of six-arm poly(ethylene glycol)-poly(3-caprolactone) (6A PEG-PCL) were developed [65]. These polymeric microparticles could reversibly switch their shapes from spherical to elliptical both extracellularly or intracellularly in with the increasing and decreasing temperature from 43°C to 0°C. The shape changing is under the mechanism of reversible 2W-SME, which should be attributed to the reversible crystalline and melting under the thermal stimuli. The phagocytosis property could be controlled by tuning the aspect ratio of the particle.

Zhu and coworkers investigated the relationship between surface textures of polymer microparticles and their drug release property [72]. Poly(D,L-lactic-co-glycolide) (PLGA) and PLGA-b-poly(ethylene glycol) (PLGA-b-PEG) microparticles with uniform size and tunable surface structures were synthesized via the process combining the advantages of interfacial instabilities of emulsion droplet and polymer-blending strategy utilizing microfluidic technology. Solvent removal from the emulsion droplets is responsible for the interfacial instabilities and the appearance of proportions. The surface roughness of the particles could be adjusted by regulating the ratio of PLGAb-PEG and PLGA in the blend, which determines the efficiency of drug loading and release kinetics of encapsulated hydrophobic paclitaxel. The particles with various roughness performed well cell viability and biocompatibility, showing the great potential in the area of fields of drug delivery and other biomedical applications.

Entanglement-based thermoplastic shape memory microparticles composed of poly(D,L-lactic acid) (PDLLA) and gold nanoparticles (Au@PDLLA hybrid microparticles) were developed (Figure 9) [70]. The shape-memory effect of the microparticles were indicated by their capability of keeping anisotropic shape at 37°C and recovery to a spherical shape at a temperature ranges from 37 to 45°C. By carefully regulating the stretching temperature, the property of shape memory and anisotropy could be imparted in the particles. The light-responsive nature of the gold nanoparticles encapsulated in the matrix provides the microparticles excellent spatiotemporal control of shape recovery for the photothermal heating. This shape memory system indicated promising potential for shape-switching drug delivery vehicles.

4. SMP Fibers at Micro-/Nanoscale

Another candidate SMP objects at micro/nanoscale to achieve the cyclic, thermomechanical test could be SMP micro/nanofibers, which can be produced by electrospinning [93–96]

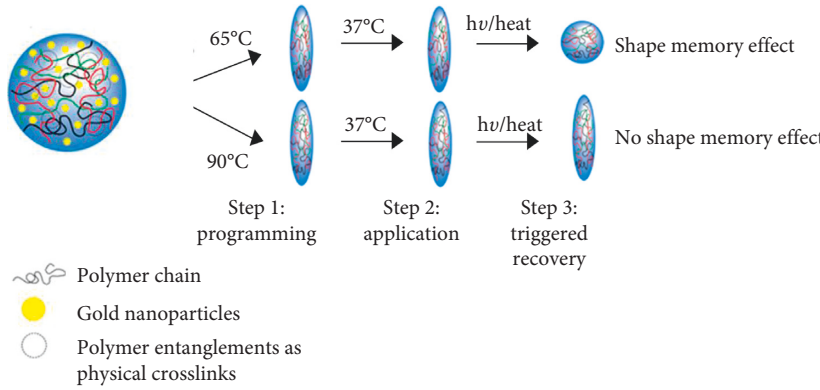

Figure 9: The structure of entanglement-based polymer microparticles and the their photothermal actuation. This figure was modified from [70].

or wet spinning [97, 98]. The shape-memory effect of fiber woven is usually investigated, and the woven can be used in smart textiles [99, 100] or biomedical fields [101, 102]. Although the SME of SMP woven is determined by knitted micro/nanofibers, physical entanglement and chemical connection play important roles as well. Therefore, the SME of a single micro/nanofiber is discussed here.

Regarding to the cyclic, thermodynamic test, the usage of atomic force microscopy (AFM) due to its high spatial resolution and force-sensing capabilities to obtain the modulus of polymer micro/nanofibers via the manner of three-point bending test has been fully developed in these decades [103–105]. This method enables an AFM cantilever tip to manipulate only a single polymer fiber, which suspends over a small trench, by applying a known force on its midpoint. Furthermore, with the combination of a hot stage, AFM can also allow a real-time investigation of polymer structures and properties while changing the temperature, which is also required for the cyclic, thermodynamic test [106, 107]. Fang et al. reported an AFM-based method that can apply the cyclic, thermomechanical test onto single, free-suspended polymer micro/nanofibers of aliphatic polyetherurethane, while unambiguously quantifying the full spectrum of their SMEs [48]. An AFM cantilever was used to program and fix a single free-suspended PEU fiber at the scale of $\approx 1\,\mu$m to a temporarily vertically bended shape. Subsequently, the stress-free and constant-strain recoveries of such programmed PEU microfiber were characterized in the real-time manner to thoroughly quantify the important characteristics of SMEs, while the temperature-memory effects (TMEs) of a single PEU microfiber were also examined. More importantly, this method was further modified to be performed onto PEU fibers at the scale of ≈ 100 nm, as well as to quantify their real-time constant-strain recoveries. The restoration of the original free-suspended shape with programming strains of $10 \pm 1\%$ and $21 \pm 1\%$ were realized upon heating [48].

Very recently, Poulin et al. developed shape memory nanocomposite fibers to use as untethered high-energy microengines [108]. Fibers were twisted at the temperature above T_g, and the mechanical deformation was stored via rapid quenching. Upon heating, the fibers generated a gravimetric work capacity that is 60 times higher than that of natural skeletal muscles due *o* high torque with large angles of rotation.

5. Summary

The development of surface structures, particles, and fibers of SMPs at micro- and nanoscale expands the application fields of SMPs in cell culture substrates, switchable valves, and channels in microfluidics, dry adhesion, optical devices, drug delivery carriers, etc. The research to date has confirmed that SME of polymers with suitable chemical structures can be achieved at nanoscale and is similar to that at macroscale. Different shape-memory effects, including temporary memory effect, reversible shape-memory effect, and multishape effect, can also be realized. The preparations of permanent surface structures, particles, and fibers of SMPs are determined by conventional approaches, while SMCPs should be concerned to create temporary shapes of large amount of polymer surface structures and particles at micro- and nanoscale simultaneously. The observation and characterization of SME are still limited by microscopy techniques. The recovery of structures is relatively easy to record. The force variation during recovery now is still a big challenge. This field is still in progress, especially SMP particles. New functions should be included in SMP particles to satisfy different requirements.

Conflicts of Interest

The authors declare that they have no conflicts of interest.

Acknowledgments

This work was supported by the National Natural Science Foundation of China (nos. 21604037 and 51503098). The Priority Academic Program Development of the Jiangsu Higher Education Institutions (PAPD) is appreciated.

References

[1] A. Lendlein and S. Kelch, "Shape-memory polymers," *Angewandte Chemie International Edition*, vol. 41, no. 12, pp. 2034–2057, 2002.

[2] Y. Liu, H. Lv, X. Lan, J. Leng, and S. Du, "Review of electro-active shape-memory polymer composite," *Composites Science and Technology*, vol. 69, no. 13, pp. 2064–2068, 2009.

[3] T. Xie, "Tunable polymer multi-shape memory effect," *Nature*, vol. 464, no. 7286, pp. 267–270, 2010.

[4] Q. Zhao, H. J. Qi, and T. Xie, "Recent progress in shape memory polymer: new behavior, enabling materials, and mechanistic understanding," *Progress in Polymer Science*, vol. 49-50, pp. 79–120, 2015.

[5] K. Hearon, M. A. Wierzbicki, L. D. Nash et al., "A processable shape memory polymer system for biomedical applications," *Advanced Healthcare Materials*, vol. 4, no. 9, pp. 1386–1398, 2015.

[6] B. Q. Y. Chan, Z. W. K. Low, S. J. W. Heng, S. Y. Chan, C. Owh, and X. J. Loh, "Recent advances in shape memory soft materials for biomedical applications," *ACS Applied Materials & Interfaces*, vol. 8, no. 16, pp. 10070–10087, 2016.

[7] A. Biswas, A. P. Singh, D. Rana, V. K. Aswal, and P. Maiti, "Biodegradable toughened nanohybrid shape memory polymer for smart biomedical applications," *Nanoscale*, vol. 10, no. 21, pp. 9917–9934, 2018.

[8] Y. Liu, H. Du, L. Liu, and J. Leng, "Shape memory polymers and their composites in aerospace applications: a review," *Smart Materials and Structures*, vol. 23, no. 2, Article ID 023001, 2014.

[9] J. Hu and S. Chen, "A review of actively moving polymers in textile applications," *Journal of Materials Chemistry*, vol. 20, no. 17, pp. 3346–3355, 2010.

[10] D. J. Maitland, M. F. Metzger, D. Schumann, A. Lee, and T. S. Wilson, "Photothermal properties of shape memory polymer micro-actuators for treating stroke," *Lasers in Surgery and Medicine*, vol. 30, no. 1, pp. 1–11, 2002.

[11] M. Behl, K. Kratz, U. Noechel, T. Sauter, and A. Lendlein, "Temperature-memory polymer actuators," *Proceedings of the National Academy of Sciences*, vol. 110, no. 31, pp. 12555–12559, 2013.

[12] H. Gao, J. Li, F. Zhang, Y. Liu, and J. Leng, "The research status and challenges of shape memory polymer-based flexible electronics," *Materials Horizons*, vol. 6, no. 5, pp. 931–944, 2019.

[13] T. Sauter, M. Heuchel, K. Kratz, and A. Lendlein, "Quantifying the shape-memory effect of polymers by cyclic thermomechanical tests," *Polymer Reviews*, vol. 53, no. 1, pp. 6–40, 2013.

[14] C. Liu, H. Qin, and P. T. Mather, "Review of progress in shape-memory polymers," *Journal of Materials Chemistry*, vol. 17, no. 16, pp. 1543–1558, 2007.

[15] S. Sun and P. Wu, "A one-step strategy for thermal- and pH-responsive graphene oxide interpenetrating polymer hydrogel networks," *Journal of Materials Chemistry*, vol. 21, no. 12, pp. 4095–4097, 2011.

[16] S. Jin, M. Liu, S. Chen, and C. Gao, "Synthesis, characterization and the rapid response property of the temperature responsive PVP-g-PNIPAM hydrogel," *European Polymer Journal*, vol. 44, no. 7, pp. 2162–2170, 2008.

[17] P. Gupta, K. Vermani, and S. Garg, "Hydrogels: from controlled release to pH-responsive drug delivery," *Drug Discovery Today*, vol. 7, no. 10, pp. 569–579, 2002.

[18] Y. Yu, M. Nakano, and T. Ikeda, "Directed bending of a polymer film by light," *Nature*, vol. 425, no. 6954, p. 145, 2003.

[19] J.-A. Lv, Y. Liu, J. Wei, E. Chen, L. Qin, and Y. Yu, "Photocontrol of fluid slugs in liquid crystal polymer microactuators," *Nature*, vol. 537, no. 7619, pp. 179–184, 2016.

[20] Y. Yu and T. Ikeda, "Soft actuators based on liquid-crystalline elastomers," *Angewandte Chemie International Edition*, vol. 45, no. 33, pp. 5416–5418, 2006.

[21] J. Hu, Y. Zhu, H. Huang, and J. Lu, "Recent advances in shape-memory polymers: structure, mechanism, functionality, modeling and applications," *Progress in Polymer Science*, vol. 37, no. 12, pp. 1720–1763, 2012.

[22] Q. Zhao, M. Behl, and A. Lendlein, "Shape-memory polymers with multiple transitions: complex actively moving polymers," *Soft Matter*, vol. 9, no. 6, pp. 1744–1755, 2013.

[23] T. Altebaeumer, B. Gotsmann, H. Pozidis, A. Knoll, and U. Duerig, "Nanoscale shape-memory function in highly cross-linked polymers," *Nano Letters*, vol. 8, no. 12, pp. 4398–4403, 2008.

[24] N. Liu, Q. Xie, W. M. Huang, S. J. Phee, and N. Q. Guo, "Formation of micro protrusion arrays atop shape memory polymer," *Journal of Micromechanics and Microengineering*, vol. 18, no. 2, Article ID 027001, 2008.

[25] N. Liu, W. M. Huang, S. J. Phee, H. Fan, and K. L. Chew, "A generic approach for producing various protrusive shapes on different size scales using shape-memory polymer," *Smart Materials and Structures*, vol. 16, no. 6, pp. N47–N50, 2007.

[26] J. T. Fulcher, Y. C. Lu, G. P. Tandon, and D. C. Foster, "Thermomechanical characterization of shape memory polymers using high temperature nanoindentation," *Polymer Testing*, vol. 29, no. 5, pp. 544–552, 2010.

[27] B. A. Nelson, W. P. King, and K. Gall, "Shape recovery of nanoscale imprints in a thermoset "shape memory" polymer," *Applied Physics Letters*, vol. 86, no. 10, Article ID 103108, 2005.

[28] Z. Fakhraai and J. A. Forrest, "Measuring the surface dynamics of glassy polymers," *Science*, vol. 319, no. 5863, pp. 600–604, 2008.

[29] J. Li, J. Shim, J. Deng et al., "Switching periodic membranes via pattern transformation and shape memory effect," *Soft Matter*, vol. 8, no. 40, pp. 10322–10328, 2012.

[30] C.-M. Chen, C.-L. Chiang, C.-L. Lai, T. Xie, and S. Yang, "Buckling-based strong dry adhesives via interlocking," *Advanced Functional Materials*, vol. 23, no. 30, pp. 3813–3823, 2013.

[31] C.-M. Chen and S. Yang, "Directed water shedding on high-aspect-ratio shape memory polymer micropillar arrays," *Advanced Materials*, vol. 26, no. 8, pp. 1283–1288, 2014.

[32] M. Ebara, K. Uto, N. Idota, J. M. Hoffman, and T. Aoyagi, "Shape-memory surface with dynamically tunable nanogeometry activated by body heat," *Advanced Materials*, vol. 24, no. 2, pp. 273–278, 2012.

[33] M. Ebara, K. Uto, N. Idota, J. M. Hoffman, and T. Aoyagi, "Rewritable and shape-memory soft matter with dynamically tunable microchannel geometry in a biological temperature range," *Soft Matter*, vol. 9, no. 11, pp. 3074–3080, 2013.

[34] Y. Jiang, U. Mansfeld, L. Fang, K. Kratz, and A. Lendlein, "Temperature-induced evolution of microstructures on poly [ethylene-co-(vinyl acetate)] substrates switches their underwater wettability," *Materials & Design*, vol. 163, Article ID 107530, 2019.

[35] J. K. Park and S. Kim, "Droplet manipulation on a structured shape memory polymer surface," *Lab on a Chip*, vol. 17, no. 10, pp. 1793–1801, 2017.

[36] Y. Wang, H. Lai, Z. Cheng et al., "Gecko toe pads inspired in situ switchable superhydrophobic shape memory adhesive film," *Nanoscale*, vol. 11, no. 18, pp. 8984–8993, 2019.

[37] W. L. Lee and H. Y. Low, "Geometry-and length scale-dependent deformation and recovery on micro-and nanopatterned shape memory polymer surfaces," *Scientific Reports*, vol. 6, p. 23686, 2016.

[38] T. Lv, Z. Cheng, E. Zhang, H. Kang, Y. Liu, and L. Jiang, "Self-restoration of superhydrophobicity on shape memory polymer arrays with both crushed microstructure and

damaged surface chemistry," *Small*, vol. 13, no. 4, Article ID 1503402, 2017.

[39] Z. Cheng, D. Zhang, T. Lv et al., "Superhydrophobic shape memory polymer arrays with switchable isotropic/anisotropic wetting," *Advanced Functional Materials*, vol. 28, no. 7, Article ID 1705002, 2018.

[40] T. Lv, Z. Cheng, D. Zhang et al., "Superhydrophobic surface with shape memory micro/nanostructure and its application in rewritable chip for droplet storage," *ACS Nano*, vol. 10, no. 10, pp. 9379–9386, 2016.

[41] S. Schauer, T. Meier, M. Reinhard et al., "Tunable diffractive optical elements based on shape-memory polymers fabricated via hot embossing," *ACS Applied Materials & Interfaces*, vol. 8, no. 14, pp. 9423–9430, 2016.

[42] C. A. Tippets, Q. Li, Y. Fu et al., "Dynamic optical gratings accessed by reversible shape memory," *ACS Applied Materials & Interfaces*, vol. 7, no. 26, pp. 14288–14293, 2015.

[43] A. Espinha, M. C. Serrano, Á. Blanco, and C. López, "Thermoresponsive shape-memory photonic nanostructures," *Advanced Optical Materials*, vol. 2, no. 6, pp. 516–521, 2014.

[44] K. Uto and M. Ebara, "Magnetic-responsive microparticles that switch shape at 37°C," *Applied Sciences*, vol. 7, no. 11, p. 1203, 2017.

[45] C. Wischke and A. Lendlein, "Method for preparation, programming, and characterization of miniaturized particulate shape-memory polymer matrices," *Langmuir*, vol. 30, no. 10, pp. 2820–2827, 2014.

[46] C. Wischke, M. Schossig, and A. Lendlein, "Shape-memory effect of micro-/nanoparticles from thermoplastic multiblock copolymers," *Small*, vol. 10, no. 1, pp. 83–87, 2014.

[47] Y. Liu, M. Y. Razzaq, T. Rudolph, L. Fang, K. Kratz, and A. Lendlein, "Two-level shape changes of polymeric microcuboids prepared from crystallizable copolymer networks," *Macromolecules*, vol. 50, no. 6, pp. 2518–2527, 2017.

[48] L. Fang, O. E. C. Gould, L. Lysyakova et al., "Implementing and quantifying the shape-memory effect of single polymeric micro/nanowires with an atomic force microscope," *ChemPhysChem*, vol. 19, no. 16, pp. 2078–2084, 2018.

[49] S. Tawfick, M. De Volder, D. Copic et al., "Engineering of micro- and nanostructured surfaces with anisotropic geometries and properties," *Advanced Materials*, vol. 24, no. 13, pp. 1628–1674, 2012.

[50] D. M. Le, K. Kulangara, A. F. Adler, K. W. Leong, and V. S. Ashby, "Dynamic topographical control of mesenchymal stem cells by culture on responsive poly(ϵ-caprolactone) surfaces," *Advanced Materials*, vol. 23, no. 29, pp. 3278–3283, 2011.

[51] Z. Wang, C. Hansen, Q. Ge et al., "Programmable, pattern-memorizing polymer surface," *Advanced Materials*, vol. 23, no. 32, pp. 3669–3673, 2011.

[52] J. D. Eisenhaure, T. Xie, S. Varghese, and S. Kim, "Microstructured shape memory polymer surfaces with reversible dry adhesion," *ACS Applied Materials & Interfaces*, vol. 5, no. 16, pp. 7714–7717, 2013.

[53] H. Xu, C. Yu, S. Wang, V. Malyarchuk, T. Xie, and J. A. Rogers, "Deformable, programmable, and shape-memorizing micro-optics," *Advanced Functional Materials*, vol. 23, no. 26, pp. 3299–3306, 2013.

[54] S. A. Turner, J. Zhou, S. S. Sheiko, and V. S. Ashby, "Switchable micropatterned surface topographies mediated by reversible shape memory," *ACS Applied Materials & Interfaces*, vol. 6, no. 11, pp. 8017–8021, 2014.

[55] S. Jeon, J. Jang, J. Youn, J.-H. Jeong, H. Brenner, and Y. S. Song, "Fullerene embedded shape memory nanolens array," *Scientific Reports*, vol. 3, no. 1, p. 3269, 2013.

[56] W. Li, T. Gong, H. Chen, L. Wang, J. Li, and S. Zhou, "Tuning surface micropattern features using a shape memory functional polymer," *RSC Advances*, vol. 3, no. 25, pp. 9865–9874, 2013.

[57] S. Reddy, E. Arzt, and A. del Campo, "Bioinspired surfaces with switchable adhesion," *Advanced Materials*, vol. 19, no. 22, pp. 3833–3837, 2007.

[58] K. A. Davis, K. A. Burke, P. T. Mather, and J. H. Henderson, "Dynamic cell behavior on shape memory polymer substrates," *Biomaterials*, vol. 32, no. 9, pp. 2285–2293, 2011.

[59] S. Kim, M. Sitti, T. Xie, and X. Xiao, "Reversible dry microfibrillar adhesives with thermally controllable adhesion," *Soft Matter*, vol. 5, no. 19, pp. 3689–3693, 2009.

[60] Q. Xu, M. Hashimoto, T. T. Dang et al., "Preparation of monodisperse biodegradable polymer microparticles using a microfluidic flow-focusing device for controlled drug delivery," *Small*, vol. 5, no. 13, pp. 1575–1581, 2009.

[61] J. Guan, A. Chakrapani, and D. J. Hansford, "Polymer microparticles fabricated by soft lithography," *Chemistry of Materials*, vol. 17, no. 25, pp. 6227–6229, 2005.

[62] S. Mawson, M. Z. Yates, M. L. O'Neil, and K. P. Johnston, "Stabilized polymer microparticles by precipitation with a compressed fluid antisolvent. 2. Poly(propylene oxide)- and poly(butylene oxide)-based copolymers," *Langmuir*, vol. 13, no. 6, pp. 1519–1528, 1997.

[63] C. Amiet-Charpentier, J. P. Benoit, P. Gadille, and J. Richard, "Preparation of rhizobacteria-containing polymer microparticles using a complex coacervation method," *Colloids and Surfaces A: Physicochemical and Engineering Aspects*, vol. 144, no. 1–3, pp. 179–190, 1998.

[64] N. Bock, M. A. Woodruff, D. W. Hutmacher, and T. R. Dargaville, "Electrospraying, a reproducible method for production of polymeric microspheres for biomedical applications," *Polymers*, vol. 3, no. 1, pp. 131–149, 2011.

[65] T. Gong, K. Zhao, W. Wang, H. Chen, L. Wang, and S. Zhou, "Thermally activated reversible shape switch of polymer particles," *Journal of Materials Chemistry B*, vol. 2, no. 39, pp. 6855–6866, 2014.

[66] Q. Zhang, T. Sauter, L. Fang, K. Kratz, and A. Lendlein, "Shape-memory capability of copolyetheresterurethane microparticles prepared via electrospraying," *Macromolecular Materials and Engineering*, vol. 300, no. 5, pp. 522–530, 2015.

[67] S. M. Brosnan, A.-M. S. Jackson, Y. Wang, and V. S. Ashby, "Shape memory particles capable of controlled geometric and chemical asymmetry made from aliphatic polyesters," *Macromolecular Rapid Communications*, vol. 35, no. 19, pp. 1653–1660, 2014.

[68] J. P. Rolland, B. W. Maynor, L. E. Euliss, A. E. Exner, G. M. Denison, and J. M. DeSimone, "Direct fabrication and harvesting of monodisperse, shape-specific nanobiomaterials," *Journal of the American Chemical Society*, vol. 127, no. 28, pp. 10096–10100, 2005.

[69] Y. Wang, T. J. Merkel, K. Chen, C. A. Fromen, D. E. Betts, and J. M. DeSimone, "Generation of a library of particles having controlled sizes and shapes via the mechanical elongation of master templates," *Langmuir*, vol. 27, no. 2, pp. 524–528, 2011.

[70] Q. Guo, C. J. Bishop, R. A. Meyer et al., "Entanglement-based thermoplastic shape memory polymeric particles with photothermal actuation for biomedical applications," *ACS*

Applied Materials & Interfaces, vol. 10, no. 16, pp. 13333–13341, 2018.

[71] L. M. Cox, J. P. Killgore, Z. Li et al., "Influences of substrate adhesion and particle size on the shape memory effect of polystyrene particles," *Langmuir*, vol. 32, no. 15, pp. 3691–3698, 2016.

[72] M. Hussain, J. Xie, Z. Hou et al., "Regulation of drug release by tuning surface textures of biodegradable polymer microparticles," *ACS Applied Materials & Interfaces*, vol. 9, no. 16, pp. 14391–14400, 2017.

[73] V. Kozlovskaya, B. Xue, and E. Kharlampieva, "Shape-adaptable polymeric particles for controlled delivery," *Macromolecules*, vol. 49, no. 22, pp. 8373–8386, 2016.

[74] J. A. Champion, Y. K. Katare, and S. Mitragotri, "Particle shape: a new design parameter for micro- and nanoscale drug delivery carriers," *Journal of Controlled Release*, vol. 121, no. 1-2, pp. 3–9, 2007.

[75] E. Eyiler and K. B. Walters, "Magnetic iron oxide nanoparticles grafted with poly(itaconic acid)-block-poly(N-isopropylacrylamide)," *Colloids and Surfaces A: Physicochemical and Engineering Aspects*, vol. 444, pp. 321–325, 2014.

[76] B. Malile and J. I. L. Chen, "Morphology-based plasmonic nanoparticle sensors: controlling etching kinetics with target-responsive permeability gate," *Journal of the American Chemical Society*, vol. 135, no. 43, pp. 16042–16045, 2013.

[77] S. Shi, Q. Wang, T. Wang, S. Ren, Y. Gao, and N. Wang, "Thermo-, pH-, and light-responsive poly(N-isopropylacrylamide-co-methacrylic acid)-Au hybrid microgels prepared by the in situ reduction method based on Au-thiol chemistry," *The Journal of Physical Chemistry B*, vol. 118, no. 25, pp. 7177–7186, 2014.

[78] Y. Pei, A. B. Lowe, and P. J. Roth, "Stimulus-responsive nanoparticles and associated (reversible) polymorphism via polymerization induced self-assembly (PISA)," *Macromolecular Rapid Communications*, vol. 38, no. 1, Article ID 1600528, 2017.

[79] L. Y. T. Chou, F. Song, and W. C. W. Chan, "Engineering the structure and properties of DNA-nanoparticle superstructures using polyvalent counterions," *Journal of the American Chemical Society*, vol. 138, no. 13, pp. 4565–4572, 2016.

[80] S. P. Meaney, B. Follink, and R. F. Tabor, "Synthesis, characterization, and applications of polymer-silica core-shell microparticle capsules," *ACS Applied Materials & Interfaces*, vol. 10, no. 49, pp. 43068–43079, 2018.

[81] J. Wang, J. D. Byrne, M. E. Napier, and J. M. DeSimone, "More effective nanomedicines through particle design," *Small*, vol. 7, no. 14, pp. 1919–1931, 2011.

[82] L. Tao, W. Hu, Y. Liu, G. Huang, B. D. Sumer, and J. Gao, "Shape-specific polymeric nanomedicine: emerging opportunities and challenges," *Experimental Biology and Medicine*, vol. 236, no. 1, pp. 20–29, 2011.

[83] L. Peponi, I. Navarro-Baena, A. Sonseca, E. Gimenez, A. Marcos-Fernandez, and J. M. Kenny, "Synthesis and characterization of PCL-PLLA polyurethane with shape memory behavior," *European Polymer Journal*, vol. 49, no. 4, pp. 893–903, 2013.

[84] H. Zhang, H. Wang, W. Zhong, and Q. Du, "A novel type of shape memory polymer blend and the shape memory mechanism," *Polymer*, vol. 50, no. 6, pp. 1596–1601, 2009.

[85] B. Alvarado-Tenorio, A. Romo-Uribe, and P. T. Mather, "Microstructure and phase behavior of POSS/PCL shape memory nanocomposites," *Macromolecules*, vol. 44, no. 14, pp. 5682–5692, 2011.

[86] H. Qin and P. T. Mather, "Combined one-way and two-way shape memory in a glass-forming nematic network," *Macromolecules*, vol. 42, no. 1, pp. 273–280, 2009.

[87] J. Li, W. R. Rodgers, and T. Xie, "Semi-crystalline two-way shape memory elastomer," *Polymer*, vol. 52, no. 23, pp. 5320–5325, 2011.

[88] T. Chung, A. Romo-Uribe, and P. T. Mather, "Two-way reversible shape memory in a semicrystalline network," *Macromolecules*, vol. 41, no. 1, pp. 184–192, 2008.

[89] K. Wang, Y.-G. Jia, C. Zhao, and X. X. Zhu, "Multiple and two-way reversible shape memory polymers: design strategies and applications," *Progress in Materials Science*, vol. 105, Article ID 100572, 2019.

[90] M. Behl, K. Kratz, J. Zotzmann, U. Nöchel, and A. Lendlein, "Reversible bidirectional shape-memory polymers," *Advanced Materials*, vol. 25, no. 32, pp. 4466–4469, 2013.

[91] M. Saatchi, M. Behl, U. Nöchel, and A. Lendlein, "Copolymer networks from oligo(ε-caprolactone) andn-butyl acrylate enable a reversible bidirectional shape-memory effect at human body temperature," *Macromolecular Rapid Communications*, vol. 36, no. 10, pp. 880–884, 2015.

[92] A. Biswas, V. K. Aswal, P. U. Sastry, D. Rana, and P. Maiti, "Reversible bidirectional shape memory effect in polyurethanes through molecular flipping," *Macromolecules*, vol. 49, no. 13, pp. 4889–4897, 2016.

[93] A. Shirole, J. Sapkota, E. J. Foster, and C. Weder, "Shape memory composites based on electrospun poly(vinyl alcohol) fibers and a thermoplastic polyether block Amide elastomer," *ACS Applied Materials & Interfaces*, vol. 8, no. 10, pp. 6701–6708, 2016.

[94] D. Kai, M. J. Tan, M. P. Prabhakaran et al., "Biocompatible electrically conductive nanofibers from inorganic-organic shape memory polymers," *Colloids and Surfaces B: Biointerfaces*, vol. 148, pp. 557–565, 2016.

[95] M. Bao, X. Lou, Q. Zhou, W. Dong, H. Yuan, and Y. Zhang, "Electrospun biomimetic fibrous scaffold from shape memory polymer of PDLLA-co-TMC for bone tissue engineering," *ACS Applied Materials & Interfaces*, vol. 6, no. 4, pp. 2611–2621, 2014.

[96] A. Iregui, L. Irusta, O. Llorente et al., "Electrospinning of cationically polymerized epoxy/polycaprolactone blends to obtain shape memory fibers (SMF)," *European Polymer Journal*, vol. 94, pp. 376–383, 2017.

[97] S. Aslan and S. Kaplan, "Thermomechanical and shape memory performances of thermo-sensitive polyurethane fibers," *Fibers and Polymers*, vol. 19, no. 2, pp. 272–280, 2018.

[98] Q. Meng, J. Hu, Y. Zhu, J. Lu, and Y. Liu, "Polycaprolactone-based shape memory segmented polyurethane fiber," *Journal of Applied Polymer Science*, vol. 106, no. 4, pp. 2515–2523, 2007.

[99] Q. Meng, J. Hu, and Y. Zhu, "Shape-memory polyurethane/multiwalled carbon nanotube fibers," *Journal of Applied Polymer Science*, vol. 106, no. 2, pp. 837–848, 2007.

[100] S. Mondal and J. L. Hu, "Water vapor permeability of cotton fabrics coated with shape memory polyurethane," *Carbohydrate Polymers*, vol. 67, no. 3, pp. 282–287, 2007.

[101] E. Niiyama, K. Tanabe, K. Uto, A. Kikuchi, and M. Ebara, "Shape-memory nanofiber meshes with programmable cell orientation," *Fibers*, vol. 7, no. 3, p. 20, 2019.

[102] M. Tomohiro, Y. Kim, T. Aoyagi, and M. Ebara, "The design of temperature-responsive nanofiber meshes for cell storage applications," *Fibers*, vol. 5, no. 1, p. 13, 2017.

[103] M. K. Shin, S. I. Kim, S. J. Kim, S.-K. Kim, and H. Lee, "Reinforcement of polymeric nanofibers by ferritin

nanoparticles," *Applied Physics Letters*, vol. 88, no. 19, Article ID 193901, 2006.

[104] S. Shanmugham, J. Jeong, A. Alkhateeb, and D. E. Aston, "Polymer nanowire elastic moduli measured with digital pulsed force mode AFM," *Langmuir*, vol. 21, no. 22, pp. 10214–10218, 2005.

[105] B. A. Samuel, M. A. Haque, B. Yi, R. Rajagopalan, and H. C. Foley, "Mechanical testing of pyrolysed poly-furfuryl alcohol nanofibres," *Nanotechnology*, vol. 18, no. 11, Article ID 115704, 2007.

[106] J. K. Hobbs and R. A. Register, "Imaging block copolymer crystallization in real time with the atomic force microscope," *Macromolecules*, vol. 39, no. 2, pp. 703–710, 2006.

[107] L. Li, C.-M. Chan, K. L. Yeung, J.-X. Li, K.-M. Ng, and Y. Lei, "Direct observation of growth of lamellae and spherulites of a semicrystalline polymer by AFM," *Macromolecules*, vol. 34, no. 2, pp. 316–325, 2001.

[108] J. K. Yuan, "Shape memory nanocomposite fibers for untethered high-energy microengines," *Science*, vol. 365, no. 6449, pp. 155–158, 2019.